Impact seismology on terrestrial and giant planets

Philippe Lognonné, T. Kawamura

20. Impact Seismology on terrestrial and giant planets

Philippe Lognonné and Taichi Kawamura

Abstract: *Impacts on the surface of the Earth and Moon surface or atmospheric blasts from impacts in Earth's atmosphere are known to generate seismic signals, either directly related by the surface impact or by ground coupling of the atmospheric blast. Although not detected by seismometers, the impact of comet Shoemaker-Levy 9 on Jupiter also generated waves, remotely observed by the Hubble Space Telescope from Earth's orbit.*
After reviewing these different observations, including those associated with artificial impacts, we present the different models used to described impact seismic sources, either for impact on the planetary surface or blast or explosion in the atmosphere. We then address impacts frequencies and use these mass/frequency models to predict the rate of expected impacts related events on Mars. Finally, we present perspectives, including those associated with joint optical/seismic monitoring of the Moon and Mars.

1- Short review of impacts seismic records in the solar system

Impacts structures are affecting all planetary surfaces in the solar systems and especially those not resurfaced by recent tectonic processes or fast erosions. Planetary seismology and remote sensing are the unique tools to monitor the dynamic of large impacts processes and associated shock wave, in a variety of conditions, from the airless Moon to the atmospheric protected Earth.

1.1. Meteorites and bolides on Earth

The largest impact ever instrumentally recorded occurred in the early time of seismology. This is the famous great Siberian meteor (Ben-Menahem, 1975) with an energy estimated to be about 12.5 Mega-tons (1 ton of TNT = 4.185 x 10^9 J). It was recorded by two Russian seismic stations at about 1000 and 5000 km, in additions to pressure records.

The development of worldwide infrasound and seismic networks allow today the detection of much smaller impacts, down to kg size in mass. Most of these impacts are detected by their generated airwaves (see Edwards *et al.*, 2008, Edwards, 2008 for a review), either with infrasound sensors or by seismometers detecting the surface displacement generated by the airwave. This acoustic detection can be furthermore be done not only locally but also at detected at larger distances, thanks to the tropospheric waveguide (Edwards, 2011).

But the airwaves are also generating seismic waves through conversion processes at the Earth surface. This is illustrated by Figure 1, which shows the recent seismic observations made by Tauzin *et al*. (2013) following the Chelyabinsk Meteor blast of February, 15, 2013. This event generated large Rayleigh surface waves propagating between 2.7 and 3.5 km/s, with amplitudes corresponding to an event with surface waves magnitude Ms~3.7. Comparable precursor Rayleigh waves, arriving well before the atmospheric air wave, are also

found also in many of the impacts reported by Edwards *et al.* (2008) but of course with smaller amplitudes

1.2. Moon and Apollo

No atmospheric shielding nor coupling occurs on the airless Moon so the seismic signals are directly related to the impact on the ground. Natural or artificial impacts therefore constituted an important fraction of the observed sources and about one-fifth of the seismic signals detected (1753 of the 9442 identified and classified events) by the Apollo seismic network were impacts.

Artificial impacts were made through the collision on the Moon of either the Saturn IVB (SIVB) upper-stage or the Lunar Module (LM) (Figure 2). The 14 230 ± 260 kg SIVBs were impacting at 2.56±0.02 km/s while the LMs were smaller seismic source, with 2320 ±60 kg impacting at 1.68±0.02 km/s. The size of the generated crater's rim diameter predicted by scaling laws is about 30m for SIVB and 6.5 m for LM (Lognonné *et al*, 2009). These diameters are comparable to observations made by the imager of NASA's LRO spacecraft (Robinson *et al*., 2010). Most of these impacts generated large signal to noise seismic signals, even at large distances, and were crucial in the determination of the crustal thickness, as the location and precise time of the impacts were known. The impact time of Apollo 16 SIVB, due to failure of the tracking, is however unknown while its location has been recovered by LRO data.

Natural impacts were typically detected at a rate of about 150 per year with different detection rates for the Apollo stations resulting from differences in local (site) amplification (Lognonné *et al.*, 2009). This much higher rate as compared to the Earth is of course directly related to the lack of atmosphere of the Moon and therefore the lack of shielding. Natural impacts were also important for interior structure analysis, as only the geographical location (e.g. latitude and longitude) and impact time had to be determined in the seismological inversions.

Figure 3 shows typical records of a large natural impact (with a 60-70m estimated crater's diameter, Gudkova *et al*., 2010) while Figure 4 provides the typical distances and amplitudes of located impacts with the long-period Apollo channels. As we will develop later, only the momentum impulse is constrained by the measurement of the seismic signals. Assuming a 20 km/s impact velocity, Figure 4 therefore shows that the typical mass of these impacts was ranging from 10's of kg to a few 1000's of kg. Many impacts were also detected on the Apollo short-period channel, but most of the time on only one seismic station.

1.3. Jupiter and Shoemaker-Levy 9

The impacts, in July 1994, of the disrupted pieces of Shoemaker-Levy 9 (SL9) comet were considered to be large enough to generate waves potentially detectable from Earth through remote sensing. The amplitudes of signals were theoretically predicted for different masses of impactors (e.g. Lognonné *et al.* 1994). For an impact with an energy greater than 10^{21}J, peak-to-peak temperature fluctuations greater than ~0.01 K were expected for 10 mHz frequency P waves, while surface waves below 3 mHz were expected to generate fluctuations in excess of 0.01 K for impacts greater than $2 \cdot 10^{21}$J (Lognonné *et al.* 1994). No seismic wave observations were however reported for the SL9 impacts (e.g. Mosser *et al.*, 1996), putting therefore upper limits on the impact energy of

1-2 10^{21} J. Though the impacts did not generated detectable body waves, it did however produce a ring-like pattern in the Jovian atmosphere, with two rings propagating at 210 m s^{-1} and 450 m s^{-1} (Figure 5 after Hammel *et al.* 1995). These waves are probably a gravity waves propagating either in the stratosphere (Walterscheid *et al.* 2000) or in a deeper layer. For Jupiter and the SL9 observation, an enhancement by a factor 10 of the water content at the 10 bar depth (about 80 km below the 1 bar level) is necessary for explaining the observed wave-front speed (e.g. Kanamori 2004).

2- The impact seismic source

2.1 seismic source on airless planets and small bodies

On airless bodies, the impactor reaches the surface without any deceleration, releasing both its momentum and kinetic energy to the planetary surface. Impacts velocities from prograde objects are decreasing with the distance of the planet to the Sun and range from 5 km to 50 km/s. While the mean impact velocity on the Moon is ~20 km/s, the ratio with those on Mercury, Venus, the Earth and Mars are 2.16, 1.28, 1.04 and 0.54 respectively (LeFeuvre and Wieczorek, 2008). A few impactors, especially those related to comets or cometary swarms, have retrograde motions and can reach the planets with much higher velocities. In all cases, both the generated shock wave and momentum carried by ejecta must be accounted in a rigorous modelling of the seismic source.

The first way to model this seismic source is to quantify the fraction of the kinetic energy transferred into seismic waves energy, defined as the seismic efficiency. The seismic efficiency of meteorite impacts has been widely discussed, either for impacts on the Moon (Laster and Press, 1968; McGarr *et al.*, 1969; Latham *et al.*, 1970, Lognonné *et al.*, 2009), on Mars (Davis, 1993, Teanby and Wookey, 2011) or on asteroids (e.g. Richardson *et al.*, 2004). Large uncertainties are found with values ranging from 10^{-6} to 10^{-4}, which leads to one order of magnitude uncertainty in the amplitude of the generated seismic waves.

The second approach is to focus on long period seismic waves, for which the area affected by the shock waves is small enough compared to the wave's wavelength to be considered as a point source. A point force seismic source (Mc Garr *et al.*, 1969, Lognonné *et al.*, 2009) can then be used, and its time dependence can be furthermore be assumed as instantaneous for periods much larger than the typical duration of the non-linear regime of the shock wave. The seismic source is then very similar to a percussion force and can be expressed as $\mathbf{f}(x,t) = \mathbf{n}_0\, \delta(\mathbf{x}-\mathbf{x}_s)\, \Phi(t))$, where $\mathbf{n}_0$ is the point force unit vector and $\delta(\mathbf{x}-\mathbf{x}_s)$ is the 3D Dirac space function at source location. For an instantaneous impact releasing a momentum p=mv to the ground, $\Phi(t) = p\delta(t)$, where $\delta(t)$ is the Dirac delta function. For a homogeneous medium, the displacement amplitude of the P or S body waves in the far field is then proportional to $\Phi(t-r/\alpha)/[\rho r\alpha^2]$, where r is the distance, ρ the density and α the P or S seismic velocity (Aki and Richards, 2002). Note here that in contrary to quake, this displacement is not proportional to a seismic moment (in Nm), but to an impulse (in Ns).

The analysis of the seismic records of the Apollo artificial impacts have confirmed this simple approach based on linear momentum conservation: for

low velocity impacts, the amplitude is proportional to the linear momentum of the impactor, while for larger velocities it is amplified by up to a factor of 2 due to impact generated ejecta (Lognonné *et al.*, 2009). While a clear corner frequency followed by a rapid ω^{-2} decrease of the spectrum is found in most of the impact spectra (see Figure 6 for a typical spectrum associated to the record of an Apollo artificial impact), a slight increasing trend with respect to the flat displacement spectrum (up to ω, see Gudkova *et al*., 2011) is found before the corner frequency which is not predicted by a simple point force. This might be related to subsurface structure where the impact shock wave occurs, which is characterized by a large seismic velocity gradient in the first few kms depth.

2.2 seismic sources on planets with atmosphere

The recent deployment of infrasound sensors, in the frame of the Comprehensive Test Ban Treaty, has multiplied observations of sonic booms associated with the impact of small (1 kg) asteroids in Earth's atmosphere. Earth's typical rate of 3 10^{-5}-2 10^{-4} km^2/yr for 1 kg objects leads indeed to approximately 4-25 detectable events per year within 200 km of the receiver. When detected by an infrasound sensor at regional (< 200 km) distances, the associated signals are short (~0.1 sec) duration pressure pulses, with typical amplitudes ranging from 0.01-0.1 Pa for the most common events, and 0.1-1 Pa for the largest ones (Edwards, 2008).

These shock waves are generated by the deceleration of the impactor in the atmosphere. Due to the high Mach numbers the atmospheric source can be considered a line source, radiating acoustic energy cylindrically outward the impact trajectory (ReVelle, 1976). In some cases, a final disruption/explosion generates a second seismic source, radiating spherical shock waves. Last but not least, but only in a very few reported cases on Earth, the impactor reaches the surface with a terminal velocity and mass large enough to generate direct seismic waves, as for the Moon and airless bodies. Larger impacts on Earth can also be detected at larger distances, thanks to the tropospheric waveguide (Edwards, 2011).

Waves in the atmosphere transition from the shock wave regime to the weakly nonlinear and finally linear regimes. For impacts with sources at about 80 km altitude, the transition to the linear regime is at Earth's altitudes between 30 km-40 km. Below the pressure wave sees little attenuation. The geometrical decay of $D^{1/2}$ for cylindrical sources generates an attenuation of ~3/4 at the ground. This is counterbalanced by the pressure increase toward the ground with amplitude increasing by the square root ratio of the ground to 35 km pressure. This provides an amplification of $\sqrt{\frac{10^5}{700}} = 12$ at the ground. Blast pressure amplitudes are therefore about one order of magnitude larger at the Earth's surface than at 35 km altitude.

Figure 7a-d illustrates the comparisons between acoustic propagations conditions on Earth and on Mars. If similarities between Mars (from the surface up to 50 km altitude) and Earth (from 35 to 80 km altitude) are found for the density and pressure, large differences in terms of acoustic velocities (200-230 m/s for Mars, 310-380 m/s for Earth) and especially attenuation factor appear.

The later, as noted by William (2001), is several order of magnitude larger due to the specific properties of CO_2 and its molecular relaxation, which generates an absorption peak at about 100 Hz at the Martian surface, furthermore shifted toward lower frequencies when the pressure decreases with altitude.

This absorption is making the propagation of the high frequency content (e.g. for frequencies larger than 1 Hz) of the blast extremely difficult, and the only signals, expected to propagate through the atmosphere, will be at periods of 10 or a few 10s of seconds (Figure 7d). These periods corresponds to those of Rayleigh surface waves, very commonly excited by the blasts on Earth, and which propagates faster than the direct acoustic waves. As a consequence, they arrive as precursors waves on Earth's records, prior to the direct acoustic wave arrival. Such waves might therefore be excited too on Mars, but likely with tiny amplitudes as this excitation process will be reduced not only by the atmospheric attenuation but also by the lower amplitude of the pressure waves on the ground as compared to Earth.

3- Impact frequencies/amplitude relation

3.1 Lunar impact detection rate and impact Hum

The impacts rate on the Moon has been studied extensively by Oberst and Nakamura (1987, 1991) who proposed an annual rate of impacts given by the following relation:

$\text{Log}_{10}\, N = -0.99 \log_{10} E + 11{,}4$,

where N is the number of event per yr, and E is the kinetic energy in J, assuming an impact velocity of 14 km/s and a seismic coupling efficiency of 10^{-6}. This gives an energy of $10^{11.5}$ J for the largest yearly impact, equivalent to a mass of about 3500 kg. For the 7.7 years of operations of the Apollo seismic network, this puts an upper bound of 2.6 10^{12} J (about 0.62 kilotons of TNT) and a mass of about 26 tons for the largest recorded impact. The sources of these large impacts were recently estimated by Gudkova *et al.* (*2*011). The impulses found were in the range of $5x10^8$-10^9 Ns. Assuming an ejecta amplification factor of 1.5 and taking the same 14 km/s impact velocity, this leads to comparable estimations for the largest impacts, in the range of 2.3-4.6 10^{12} J. Many uncertainties remain in either the propagation condition or the seismic efficiency/source model.

For smaller impact of about 1 kg (about 10^8 J) Oberst and Nakamura rate suggests about 3000/yr. As recently shown by Lognonné *et al.* (2009) such a rate is well retrieved by a Monte-Carlo simulation of impacts constrained by the impact flux rate determined by other techniques, including classified ones based on the detection of impacts in the Earth's upper atmosphere with early warning satellites (e.g. Brown *et al*., 2002). Here again, an uncertainty of a factor of two remains due to the unknown in the propagation properties used for the Moon, including attenuation.

Finally, impacts are likely the source of the background seismic noise on airless planets like the Moon. Such bodies are expected to have a relatively low seismic noise, as their surfaces are only subject to long period, diurnal, temperature changes. However impacts (including micro impacts) occur continuously. Lognonné *et al* (2009) suggested impacts as a primary source of micro-seismic noise, with a proposed background noise ranging between 2/1000 and 2/100 of the Apollo resolution around 0.5 Hz. This might be an ultimate

limits for future lunar seismometers, although very challenging as this noise level corresponds to ground accelerations in the range of only 10^{-12}-10^{-11} m/s^2.

3.2 Expected detection rate on Mars

On Mars, both the velocity and the mass of the impactors are reduced during atmospheric entry, which can be assessed by integrating the impactor trajectory equation in the atmosphere (e.g. Lognonné and Johnson, 2007). The atmospheric shielding effect on Mars is small, comparable to the Earth at altitudes of 30km or higher (ReVelle, 1976). Figure 8a illustrates both this atmospheric shielding effect and the typical rate of events occurring during two earth years, by using a random simulation based the impactor rate model of LeFeuvre and Wieczorek (2008). The entry flux of meteorites is 2.6 times larger than for Earth-Moon due to the proximity of the asteroid belt (e.g. Davis 1993) but is balanced by the impact velocity which is about half that for Earth-Moon. The number of impacts per year detected by a seismic station on Mars might be about 10 seismic events per year with an amplitude larger than 5 x 10^{-9} m/s^2. These would be associated with impacts of objects with masses of several hundred of kg. Most of the difference between Mars and the Moon is expected to be associated with differences in crustal seismic attenuation. This attenuation is unknown for Mars but is likely less than on Earth.

3.3 Temporal and spatial variations

As impact rates and the strength of the associated seismic source depends on the distribution of the impactors with respect to the orbit of the studied body and of their terminal impact velocity, temporal variations of the impact rates as well as differences with respect to latitude and/or angular position with respect to the orbital plane are expected. On the Moon, additional effects will be related to the orbit of the Moon with respect to Earth, which generates a leading-trailing asymmetry observed on the density of craters. This enhancement on the leading side has been detected by Kawamura *et al.* (2011) in the collection of lunar impacts detected by Apollo. On Mars, 20% more impacts are expected at high latitude as compared to the equator and temporal variations are expected with the variation of the distance between Mars and the asteroid belt, up to a factor of 4-5 between the maximum flux and the minimum one during a Mars year (LeFeuvre and Wieczorek, 2008).

4- Perspectives and future

We can expect that both the future NASA InSight mission to Mars in 2016 and further planetary seismology projects on the Moon and Mars in the 2020 decade will provide new seismic observations of impacts. SL9-type impacts on Jupiter were on the other hand a unique observation: even if new smaller impacts were detected again on Jupiter (e.g. Hammel *et al*., 2010), the recurrence time of events large enough for remote sensing of seismic waves has been estimated to be 500 yrs or more (Roulston and Ahrens, 1997).

Future planetary seismic missions can leverage the possibility of observing surface impacts with both seismometers and remote sensing techniques. On the Moon, as impacts are known to generate a flash when hitting the Lunar surface (Ortiz *et al*., 2006), both time and location might be obtained. On Mars however, only the location will be obtained through the differential analysis of high

resolution imaging data taken before and after the impact (e.g. Daubar *et al.*, 2013). Complete data set will then be obtained, with location, crater size and morphology, seismic waves records for both Mars and the Moon, with moreover for the Moon the additional measurement of the impact time and flash emission spectrum. The expected number of impacts to be detected and located on Mars through seismic waves remains modest (5-10 per year depending on instrument noise) but comparable to the artificial located impact performed during Apollo. A much larger rate of observations will be possible on the Moon due to the much lower attenuation (Yamada *et al.*, 2011). High resolution seismic tomography of the lunar crust can therefore be imagined when seismometers will be deployed again on the Moon and will be coupled with lunar flash monitoring from Earth or from lunar high altitude orbit.

5- References

Aki, K. and P. G. Richards (2002). *Quantitative seismology (second edition)*, University Science books, CA, USA

Ben-Menahem, A. (1975). Source parameters of the Siberian explosion of June 30, 1908, from analysis and synthesis of seismic signal at four stations, *Phys. Earth Planet. Inter*., **11**, 1-35.

Brown, P., Spalding, R. E., ReVelle, D. O., Tagliaferri, E., Worden, S. P. (2002). The flux of small near-earth objects colliding with the Earth. *Nature*, **420**, 294-296.

Daubar, I. J., McEwen, A. S, Byrne, S, Kennedy, M R, Ivanov, B 2013 The current martian cratering rate. *Icarus*, **225**, 506-516.

Davis, P. M. (1993). Meteoroid impacts as seismic sources on Mars. *Icarus*, **105**, 469-78.

Edwards, W. N. (2008). Meteor Generated Infrasound: Theory and Observation, Chapter 12. In *Infrasound monitoring for atmospheric studies*, 355-408, Springer-verlag, New-York, A.Le Pichon editor.

Edwards, W. N., Eaton, D. W., Brown, P. G. (2008). Seismic observations of meteors: Coupling theory and observations, *Reviews of Geophysics*. **46**, CiteID RG4007.

Gudkova, T.,Lognonné, P., Gagnepain-Beyneix, J. (2011). Seismic source inversion for large impacts detected by the Apollo seismometers, *Icarus*, **211**, 1049-1065.

Hammel, H. B., Beebe, R. F., Ingersoll, A. P. *et al*. (1995). HST imaging of atmospheric phenomena created by the impact of comet Shoemaker-Levy 9. *Science*, **267**, 1288-96.

Hammel, H. B., Wong, M. H., Clarke, J. T. *et al*. (2010). Jupiter after the 2009 impact: Hubble space telescope imaging of the impact-generated debris and its temporal evolution, *Astr. J. Lett*., **715**, L150

Kanamori, H. (2004). Some fluid-mechanical problems in geophysics-wave in the atmosphere and fault lubrification. *Fluid dynamics Res*., **34**, 1-19.

Kawamura, T., Morota, T., Kobayashi, N., Tanaka, S. (2011). Cratering asymmetry on the Moon: New insight from the Apollo Passive Seismic Experiment, *Geophys. Res. Lett*., **38**, Issue 15, CiteID L15201

Laster, S. J. and Press, F. (1968). A new estimate of lunar seismicity due to meteorite impact. *Phys. Earth Planet. Inter*., **1**, 151–154.

Latham, G. V., Ewing, M., Dorman, J. *et al*. (1970). Seismic data from man-made impacts on the moon. *Science*, **170**, 620-26.

Le Feuvre, M., Wieczorek, M. A. (2008). Nonuniform cratering of the terrestrial planets. *Icarus* **197**, 291–306.

Lognonné, P. and Johnson, C. L. (2007). Planetary seismology, *Treatrise on Geophysics*, 10:69-122., Elsevier.

Lognonné, P., Mosser, B., Dahlen, F. A. (1994). Excitation of the jovian seismic waves by the Shoemaker-Levy 9 cometary impact. *Icarus*, **110**, 180-95.

Lognonné, P, Le Feuvre, M., Johnson, C. L. and Weber, R. C. (2009). Moon meteoritic seismic hum: steady state prediction. *J. Geophys. Res*., 114, E12003.

McGarr, A. G., Latham, V. and Gault, D. E. (1969). Meteoroid impacts as sources of seismicity on the Moon. *J. Geophys. Res*., **74**, 5981– 5994.

Mosser, B., Galdemard, P., Lagage P *et al*. (1996). Impact seismology: a search primary pressure waves following impacts A and H. *Icarus*, **121**, 331-40.

Oberst, J. and Nakamura, Y. (1987). Distinct meteoroid families identified on the lunar seismograms, *J. Geophys. Res*., **92**, 769–773.

Oberst, J. and Nakamura, Y. (1991). A search for clustering among the meteoroid impacts detected by the Apollo lunar seismic network, *Icarus,* **91**, 315–325.

Ortiz, J. L., Aceituno, F. J., Quesada J., A. *et al.* (2006). Detection of sporadic impact flashes on the Moon: Implications for the luminous efficiency of hypervelocity impacts and derived terrestrial impact rates. *Icarus*, **184**, 319–326.

ReVelle, D. (1976). On meteor generated infrasound, *J. Geophys. Res.,* **81**, 1217-1229.

Richardson, J. E., Melosh, H. J. and Greenberg, R. (2004). Impact-Induced Seismic Activity on Asteroid 433 Eros: A Surface Modification Process, *Science*, **306**, 1526-1529.

Robinson, M. S., Brylow, S. M., Tschimmel et al. (2010) , Lunar Reconnaissance Orbiter Camera (LROC) Instrument Overview, *Space Science Reviews*, **150**, 81-124.

Roulston, M. S. and Ahrens, T. J. (1997). Impact Mechanics and Frequency of SL9-Type Events on Jupiter, *Icarus*, **126**, 138-147.

Tauzin, B., E. Debayle, C. Quantin, and N. Coltice (2013). Seismoacoustic coupling induced by the breakup of the 15 February 2013 Chelyabinsk meteor, *Geophys. Res. Lett*., **40**, 3522–3526.

Teanby, N. and Wookey, J. (2011). Seismic detection of meteorite impacts on Mars, *Phys. Earth Planet. Int.*, **186**, 70–80.

Walterscheid R L, Brinkman, D. G., Schubert, G. (2000). Wave disturbances from the comet SL-9 impacts into Jupiter's atmosphere, *Icarus,* **145**, 140-46

Williams, J. P. (2001). Acoustic environment of the martian surface. *J. Geophys. Res*. **106**, 5033–5041.

Yamada, R., Garcia, R. F., Lognonné, P., Le Feuvre, M., Calvet, M. and Gagnepain-Beyneix, J. (2011). Optimisation of seismic network design: Application to a geophysical international lunar network, *Planet. Space Sci*., **59**, 343-354.

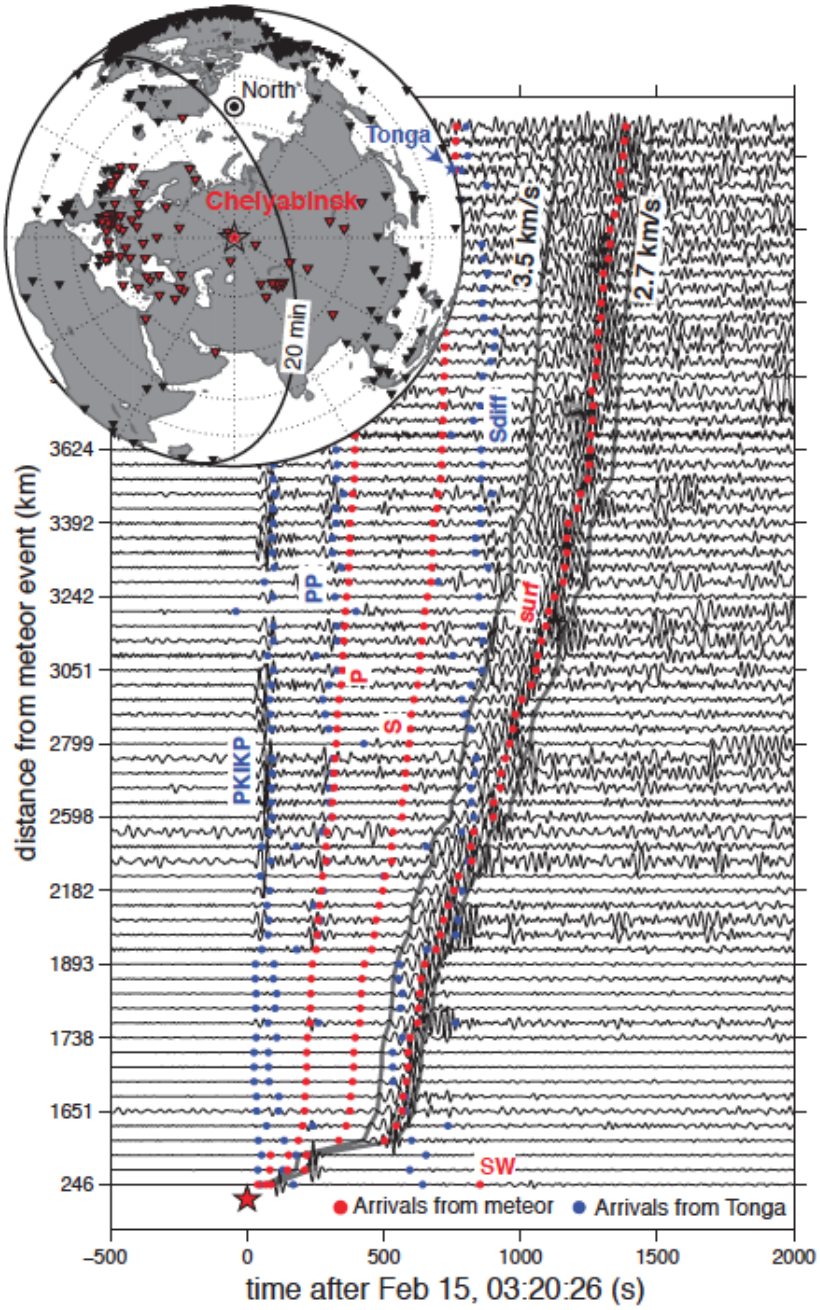

Figure 1: Bandpass filtered vertical seismograms up to 4000 km of epicentral distance, recorded after the Chelyabinsk blast. The filtering window is between 20 and 60 sec and corresponds to the surface waves bandwidth. The blue dots show the arrival of seismic waves associated with an earthquake occurring in the Tonga Islands 20 minutes before the impact. The 20 min travel time iso-contour for this earthquake is indicated on the Earth's sphere, while an arrow gives its epicentre location. (Reprinted from Tauzin *et al.*, 2013)

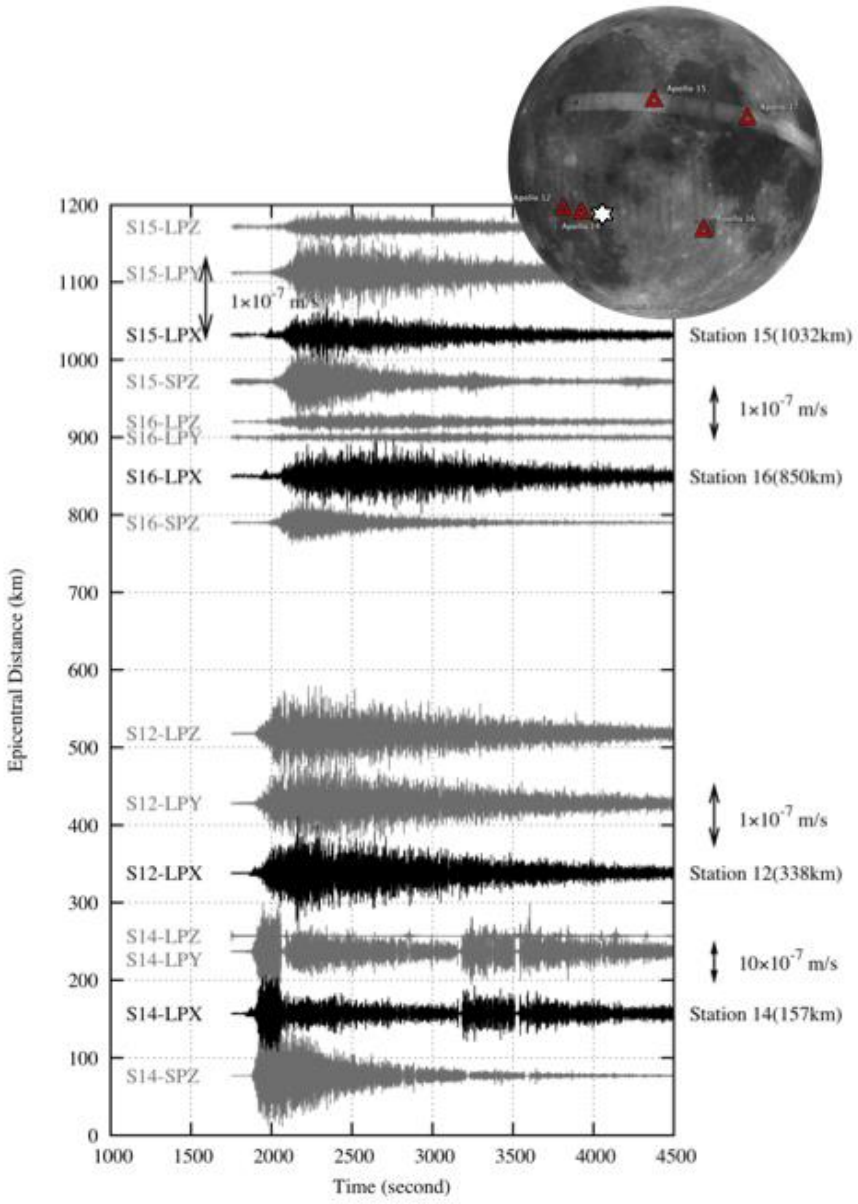

Figure 2: Ground velocity records from the Apollo seismic network, of the impact of the Apollo 17 Saturn V upper stage (Saturn IVB) on the Moon on 10 December 1972 (at distances of 338, 157, 1032 and 850 km from the Apollo 12, 14, 15 and 16 stations, respectively). Data are shown for the long-period seismometer (LPX, Y, Z) plus the vertical axis of the short-period seismometer (SPZ). Amplitudes at the Apollo 14 station, 157 km from impact, are saturated mainly due to S waves trapped in the regolith. The first P arrival is typically 10 times smaller. Note the 10-db gain change at the middle of the LPX and LPY records of station 14 who saturated for the large signal. The amplitude arrow for this station is for the amplitudes before this gain change.

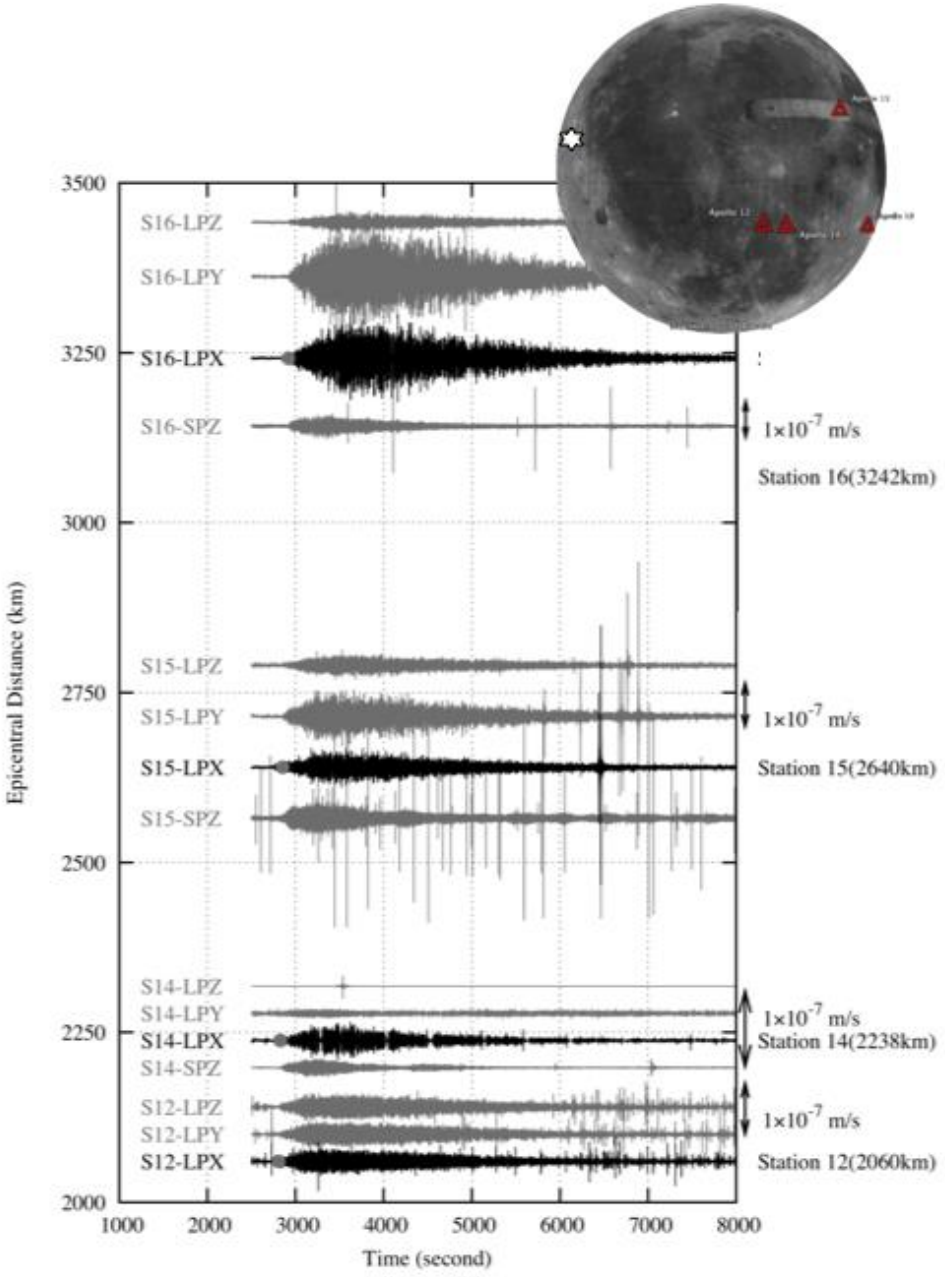

Figure 3: Typical records of the large natural impact occurring on November, 14, 1976, recorded at the Apollo stations. The same processing as for Figure 2 was done. Note that amplitudes at similar epicentral distance are larger than those of figure 1. The mass of the impact has been estimated to about 25-35 tons assuming an impact velocity of 20 km/s. The lunar globe were taken from LROC observation of NASA (http://photojournal.jpl.nasa.gov/catalog/PIA14011) and Apollo stations and deep moonquake nests were added by the authors.

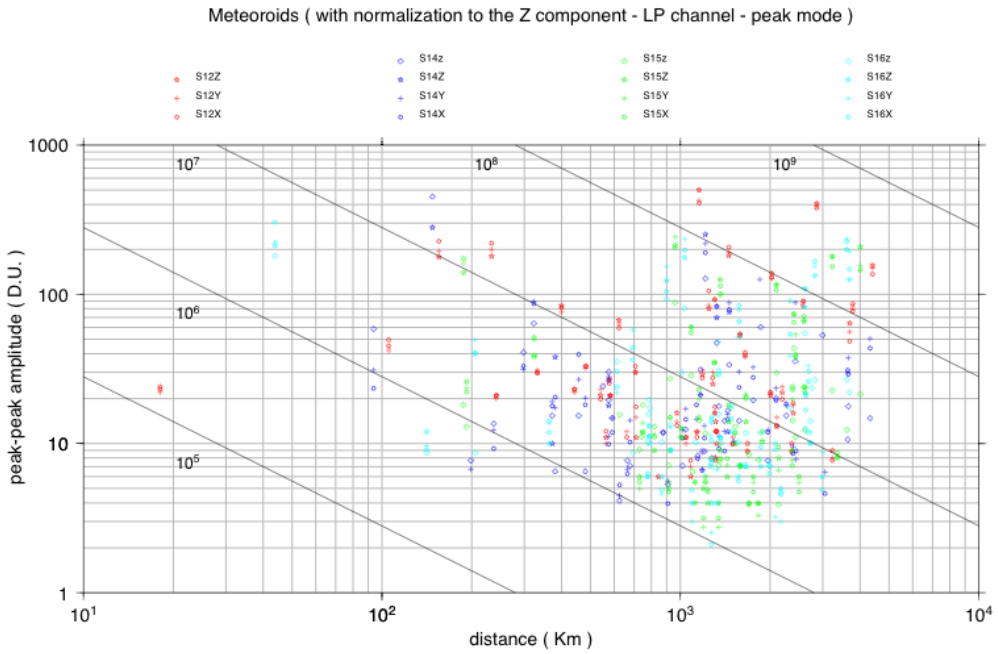

Figure 4: Peak to peak amplitudes of the impacts detected by the different Apollo channels, in DU, with respect to epicentral distance. The oblique lines are the source amplitudes, from 10^5 Ns up to 10^9 Ns in the Y direction, while the 1/D decay of the oblique lines is mainly due to geometrical spreading, as attenuation is very low on the Moon. The moments correspond to impacts from about 3 kg to 30 tons at 20 km/s velocities and with ejecta amplification of 1.5 (Reprint of Fig. 9 of Gudkova et al., 2009).

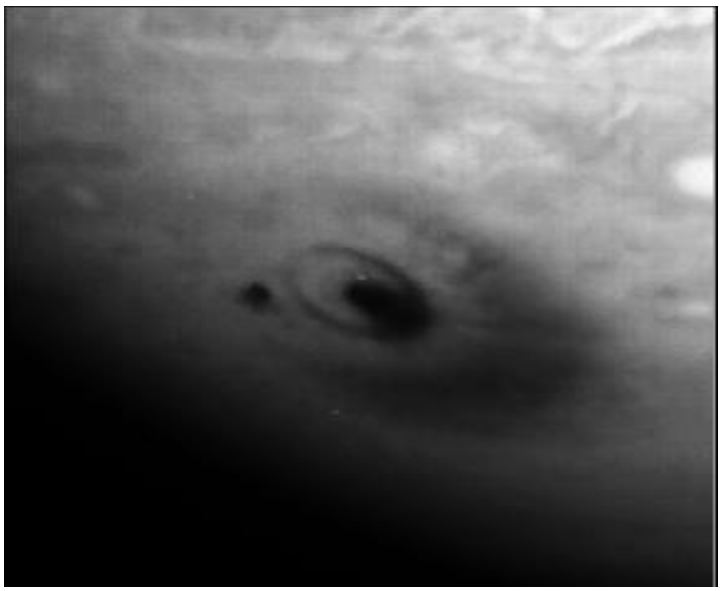

Figure 5: Wave features generated by the impact G of the Shoemaker-Levy 9. After Hammel *et al.*, 1995.

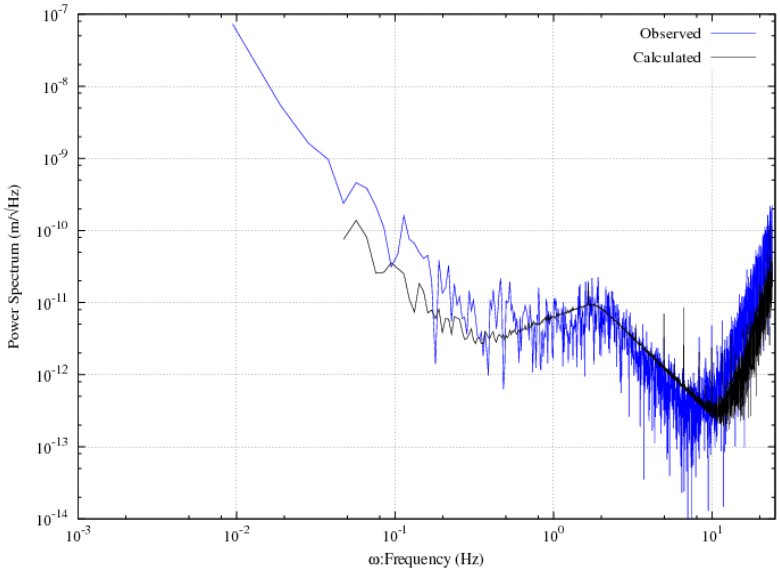

Figure 6 : Displacement spectrum of the Apollo 17 SIVB impact recorded at the Apollo station 16. The spectrum is a composite spectrum of the long-period and short-period vertical channels both corrected from the instruments transfer functions. The corner frequency is at about 2 Hz and correspond to a maximum of amplitude. The spectrum increase below 0.2 Hz and above 10 Hz are instrument noise.

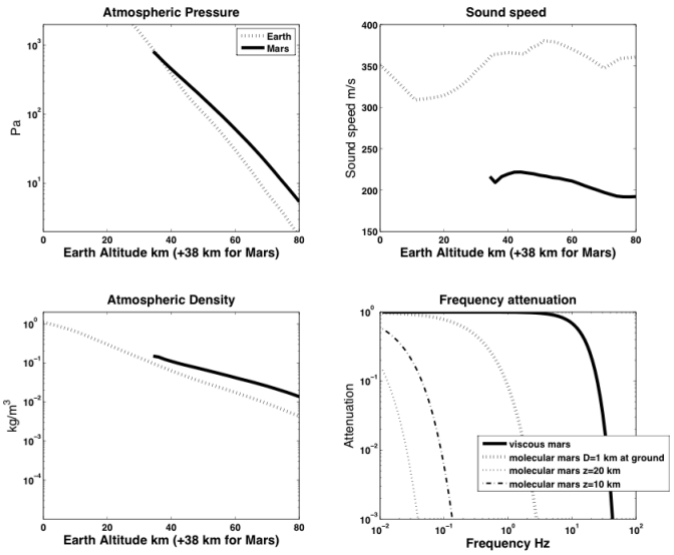

Figure 7: comparison of the acoustic condition on Mars and Earth upper atmosphere. The Mars surface pressure is approximately equal to the Earth's one at 38km of altitude, and altitudes for Mars on all curves are therefore shifted by this value. From top to bottom and left to right: Atmospheric pressure, sound speed, Atmospheric density and attenuation factor at different frequencies (the attenuation factor is the inverse of the distance in m over which the sound energy decay by e^2). The atmospheric properties are expected to experience daily

and geographical variations. From right to left and for the attenuation: the two first lines are the attenuation due to viscosity and to molecular relaxation for 1 km of propagation at the ground, showing the major impact of molecular relaxation. The long dashed and dotted line are the attenuation for sources at 10 km and 20 km altitude respectively, showing that only the very long period acoustic waves can reach the surface for blasts originating from 10-20 km altitudes.

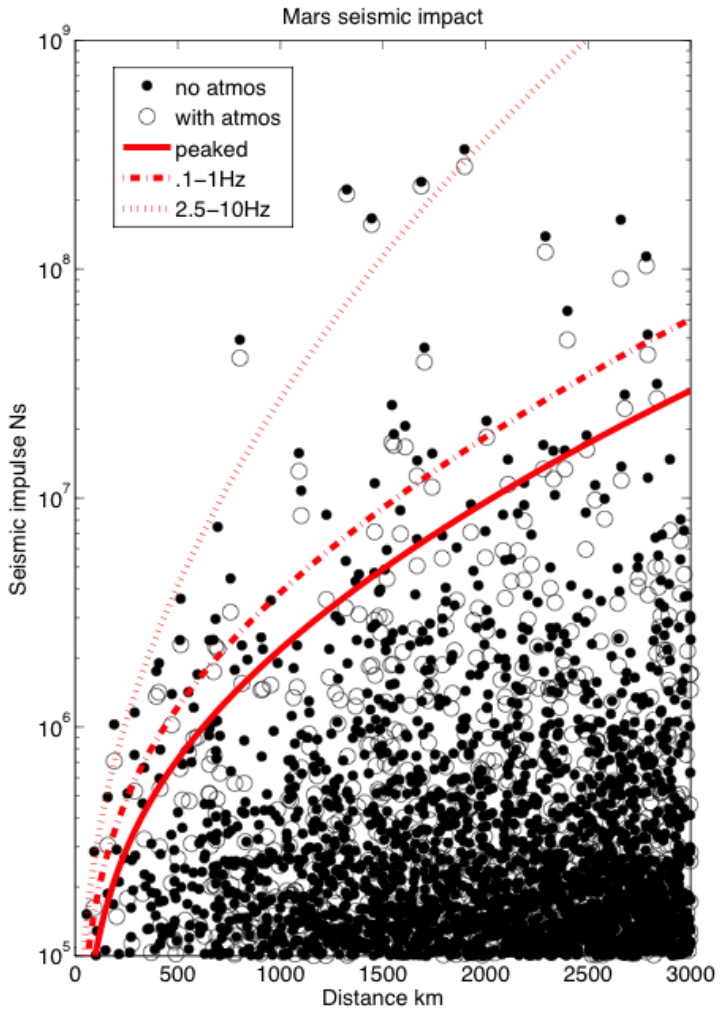

Figure 8: Random simulation of impact events, to be detected by a Mars mission during 2 earth yr of operation. The distribution of impactors has mass and velocities given by LeFeuvre and Wieczorek (2008) probabilities. The seismic amplitudes are estimated following the methods described by Lognonné et al (2009) and calibrated by using artificial Moon impact data corrected for Mars condition in the crust (Q of 600 and shear velocity of 4.5 km/s). Small dots are impacts impulse without atmospheric ablation, while circles are with atmosphere, for the same impactors population. Note that the atmospheric shielding is significant for the small ones, but marginal for the large. Lines are for detection threshold corresponding to signal to noise of 3 and flat noise levels 5 10^{-10} $ms^{-2}/Hz^{1/2}$, 10^{-8} $ms^{-2}/Hz^{1/2}$ in 0.the 1-1Hz and 1-3Hz bandwidth respectively.